doi.org/10.1002/cbdv.202301970 Research Article CHEMISTRY & BIODIVERSITY

www.cb.wiley.com

Synthesis, Characterization and Evaluation of the Antimicrobial and Herbicidal Activities of Some Transition Metal Ions Complexes with the Tranexamic Acid

Amira A. Mohamed,[a] Sadeek A. Sadeek,[b] Nihad G. Rashid,[c] Hazem S. Elshafie,[d] and Ippolito Camele*[d]

New tranexamic acid (**TXA**) complexes of ferric(III), cobalt(II), nickel(II), copper(II) and zirconium(IV) were synthesized and characterized by elemental analysis (CHN), conductimetric (Λ), magnetic susceptibility investigations (μeff), Fourier transform infrared (FT-IR), proton nuclear magnetic resonance (^{1}H-NMR), ultraviolet visible (UV-vis.), optical band gap energy (E_g) and thermal studies (TG/DTG and DTA). **TXA** complexes were established in 1 : 2 (metal: ligand) stoichiometric ratio according to CHN data. Based on FT-IR and ^{1}H-NMR data the disappeared of the carboxylic proton supported the deprotonating of **TXA** and linked to metal ions via the carboxylate group's oxygen atom as a bidentate ligand. UV-visible spectra and magnetic moment demonstrated that all chelates have geometric octahedral structures. E_g values indicated that our complexes are more electro conductive. DTA revealed presence of water molecules in inner and outer spheres of the complexes. DTA results showed that endothermic and exothermic peaks were identified in the degradation mechanisms. The ligand and metal complexes were investigated for their antimicrobial and herbicidal efficacy. The Co(II) and Ni(II) complexes showed antimicrobial activity against some tested species. The obtained results showed a promising herbicidal effect of **TXA** ligand and its metal complexes particularly copper and zirconium against the three tested plants.

Introduction

Antifibrinolytics are classes of medication that are inhibitors of fibrinolysis such as aminocaproic acid (ε-aminocaproic acid) and tranexamic acid.[1–4] Tranexamic acid (amino-methyl-cyclohexane-carboxylic acid) (**TXA**) (Scheme 1) is one of amino acid, lysine derivatives, it was first synthesized by the Japanese husband, wife team Shosuke and Utako Okamato.[5] **TXA** is widely utilized in both trauma and routine surgery to minimize excessive blood loss because of its significant antifibrinolytic action, which is attributed to the aminomethyl and carboxylic acid substituents on the cyclohexane ring occupying equatorial locations and its inhibitory effects against fibrinolysis.[6–9] **TXA** is exceedingly utilized as an antifibrinolytic drug, prohibits fibrinolysis by restricting lysine-binding sites on plasminogen, curtailing the activation of plasmin; and therefore, prevents excessive blood loss from trauma, surgery e.g., cardiac, orthopedic, liver transplantation, postpartum bleeding, nosebleeds, and heavy menstruation. **TXA** is employed in numerous surgical or medical circumstances, including cardiac, orthopedic, liver transplantation, urological, and obstetric surgery, because of its antifibrinolytic action.,[10–16] also reduce collateral effects and/or enhance the drug's action through the formation of metallic complexes.[3] A new observation was made regarding amino-methyl-cyclohexane-carboxylic acid. Nearly concurrently with a Swedish ensemble,[8] It was demonstrated that the trans-conformation exists in the antifibrinolytic active isomer. Compared to an older equivalent called e-aminocaproic acid, **TXA** has approximately eight times the antifibrinolytic action.[9] Moreover, in cases of unusual bleeding during or following surgery, aplastic anaemia, leukemia.[10] Furthermore, it discloses anti-inflammatory and skin brightening effects.[11–13] Experimental data indicate that **TXA** behaved as a bidentate ligand that coordinated to metal ions through the carboxylate group's

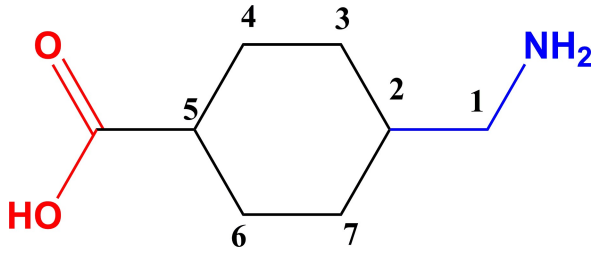

Scheme 1. 4-(Amino methyl) cyclohexane carboxylic acid tranexamic acid (**TXA**).

[a] *A. A. Mohamed*
Department of Basic Science, Zagazig Higher Institute of Engineering and Technology, Zagazig 44519, Egypt

[b] *S. A. Sadeek*
Department of Chemistry, Faculty of Science, Zagazig University, Zagazig 44519, Egypt

[c] *N. G. Rashid*
Ministry of Education, Babylon 51001, Iraq

[d] *H. S. Elshafie, I. Camele*
School of Agricultural, Forestry, Food and Environmental Sciences, University of Basilicata, Viale dell'Ateneo Lucano 10, Potenza 85100, Italy
Tel.: +39-0971-205544
Fax: +39-0971-205503
E-mail: ippolito.camele@unibas.it

Supporting information for this article is available on the WWW under https://doi.org/10.1002/cbdv.202301970

oxygen atom to generate octahedral formalization complexes.[14–22]

The intention of the present investigation was to investigate the possibility of expanding the pharmacological profile of the drug (**TXA**) in order to identify new properties like antimicrobial activity and to create new **TXA** complexes with necessary metal ions that are likely to display distinct biological behaviors from the parent drug.[4,23,24] Some new transition metal ions complexes of **TXA** were synthesized. Elemental analysis, FT-IR, ^{1} H-NMR, UV-vis, molar conductivity and magnetic susceptibility measurements, thermal analyses (TG-DTG, DTA) were used to characterize the structures of the metal complexes, antibacterial activity of the new metal complexes was investigated against three bacterial species *Bacillus megaterium, Escherichia coli, Xanthomonas campestris* and three phytopathogenic fungal species *Fusarium oxysporum, Monilinia fructicola and Penicillium italicum.* Phytotoxicity assay was also evaluated on seed germination and radical elongation (SG-RE) of *Lepidium sativum* L. (garden cress), *Lactuca sativa* L. (Lettuce), and *Solanum lycopersicum* L. (tomatoes).

2. Results and Discussion

2.1. Elemental Analysis and Molar Conductance

Elemental analyses, molecular formulae, melting points, color, percent yields of complexes, μeff and Λ of compounds were listed in Table 1. The estimated data and elemental analytical results for **TXA** metal complexes were in satisfactory agreement. Generally speaking, all complexes are soluble in DMSO and DMF and non-hygroscopic solids. Molar conductance data of the complexes in DMF solvent with standard concentration (1×10^{-3} mol^{-1}) were in the domain of 12.96–90.16 Scm^2/mol. The data adequately assured the non-electrolytic nature of the complexes except complex **(1)** which found as 1:1 electrolyte.[25–27] This actuality articulated that the chloride ion were absent from outside the coordination sphere for complexes **(2), (3) (4)** and **(5)**.[28]

2.2. FT- IR Spectra and Mode of Bonding

When a strong method like X-ray crystallography is not available, FT-IR spectra have shown to be the most useful instrument for clarifying the process of ligand attaching to metal ions. The FT-IR spectra of **TXA** and its metal complexes were plotted out *(Figure S1)* and their significant stretching frequencies were reported in Table 2. **TXA**'s infrared spectra showed two prominent broad bands at 3296 and 3150 cm^{-1}, which were attributed to the amino group's stretching vibration ν(NH_2), and at 3426 cm^{-1}, a broad band that corresponded to the carboxylic group (−COOH).[29–35] The stretching vibration of the carboxylic group's ν(C═O) has been accountable for strong band at 1641 cm^{-1}.[34,35] When the FT-IR spectra of our complexes are compared to those of **TXA**, the absence of the absorption band at 1641 cm^{-1}, which is attributed to the carboxylic group (COOH), indicates that the carboxylate group of **TXA** has been chelated with metal ions via the two oxygen atoms.[32] The symmetric vibrations (ν_s) at about 1454 cm^{-1} and the stretching asymmetry (ν_{as}) of the carboxylate group at approximately 1565 cm^{-1} verify that **TXA** is chelated with metal ions.[33–35] The $\Delta\nu$ (ν_{as}–ν_s) values for complexes lower than 200 cm^{-1} correlated a bidentate chelation mode via the carboxylate group's oxygen of the **TXA**. All complexes exhibit a broad band in 3432–3538 cm^{-1} region, indicating the presence of coordinated and hydrated water molecules in all complexes, as confirmed by elemental and thermal analytical tests.[34,36–39] Additionally, the spectra of isolated complexes revealed an assortment of bands with varying intensities that corresponded to ν(M–O) and ν(M–N) within the 667–501 cm^{-1} range.[36–39] The suggested structure formula based on the findings presented in accordance with the complexes' proposed structures as indicated in (Scheme 2).

2.3. UV-vis. Spectra and Magnetic Moment Measurements

UV-visible spectra of **TXA** and its metal complexes were reported (*Figure S2*) from 200 to 800 nm to obtain more valuable inquiry UV-visible spectral facts. The magnetic suscept-

Table 1. Elemental analysis and physico-analytical data for **TXA** and its metal complexes.

Compounds M.Wt. (M.F.)	Color Yield (%)	M.P./ °C	Calc. (Found) (%) C	H	N	M	Cl	Λ Ω cm^2 mol^{-1}	μ_{eff}(B.M.)
TXA 157.21 ($C_8H_{15}NO_2$)	White	165	59.92 (61.06)	9.46 (9.54)	8.81 (8.90)	–	–	9.12	
(1) 475.71($FeC_{16}H_{36}N_2O_8Cl$)	Reddish brown 83.24	250	40.28 (40.36)	7.48 (7.56)	5.80 (5.88)	11.61 (11.73)	7.34 (7.45)	85.16	5.63
(2) 425.35($CoC_{16}H_{34}N_2O_7$)	Violet 88.63	330	45.05 (45.13)	7.89 (7.99)	6.49 (6.58)	13.77 (13.85)		22.30	4.42
(3) 461.11($NiC_{16}H_{38}N_2O_9$)	Pale green 80.96	290	41.51 (41.63)	8.17 (8.24)	6.00 (6.07)	12.61 (12.72)		23.27	3.16
(4) 447.96($CuC_{16}H_{36}N_2O_8$)	Dark green 81.64	350	42.77 (42.86)	7.96 (8.03)	6.20 (6.25)	14.08 (14.18)		20.21	1.70
(5) 473.64($ZrC_{16}H_{34}N_2O_8$)	Light white 79.21	250	40.41 (40.53)	7.10 (7.17)	5.85 (5.91)	19.17 (19.26)		12.96	

Table 2. Selected infrared wave numbers (cm^{-1}) for **TXA** and its metal complexes.

Compounds	ν(O–H) H_2O	ν(NH_2)	ν(COO^-)	$\nu_{as}(COO^-)$	$\nu_s(COO^-)$	Δν (ν_{as}-ν_s)	**ν(M–O) and ν(M–N)**
TXA	3426wbr	3296w 3150w	1641s	—	—		—
(1)	3471s	3231m 3138m		1580vs	1450vs	130	627m and 564m
(2)	3435mbr	3200w 3152w		1579m	1456w	123	667w and 501m
(3)	3538s	3341m 3265w	—	1584s	1445s	139	620m and 582m
(4)	3432mbr	3244w 3190m	—	1575vs	1454vs	121	601m and 547w
(5)	3444s	3209w 3100vw	—	1565s	1454m	111	664m and 541w

Keys: s = strong, w = Weak, m = medium, br = broad, v = strong, ν = stretching.

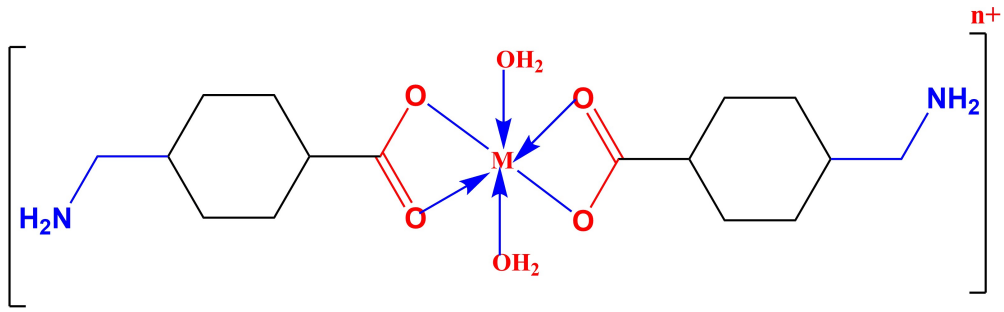

m=Fe(III), Co(II), Ni(II) and Cu(II)

n=1 For Fe(III) and 0 for Co(II), Ni(II) and Cu(II)

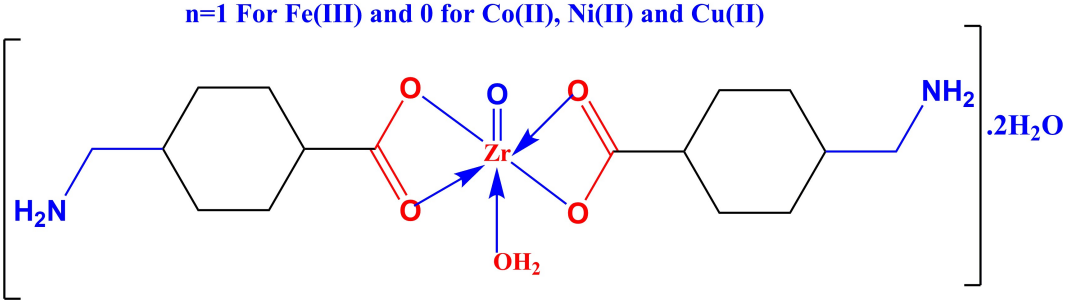

Scheme 2. Chelation mode of Fe(III), Co(II), Ni(II), Cu(II) and Zr(IV) with **TXA.**

ibility measurements of the solid complexes were done and the μ_{eff} values for Fe(III), Co(II), Ni(II) and Cu(II) complexes were found at 5.63, 4.42, 3.16 and 1.70 B.M.[31–33] The absorption bands of **TXA** were seen at 295 and 315 nm (Table 3) can be imputed to transitions of π–π* and n–π*.[34,40] Some shifts and new bands were noticed when the electronic spectrum of the free **TXA** were compared to those of spectra corresponding to metal complexes, this can be used as proof of the complex formation. The spectra of metal complexes reveal many bands at various wavelengths each of which corresponds to a particular transition implying the geometry of the complexes. The new bands in the spectra of complexes were typed in the range 21052–22471 cm^{-1} which assigned to ligand metal charge transfer (LMCT).[41–43] The Fe(III) chelate UV-vis spectrum shows a band at 18181 cm^{-1} that might be related to $^6A_{1g}$-$^4T_{2g}$ transition in octahedral geometry with 10Dq 358 kj/mol with crystal field stabilization energy (CFSE) −573 + p,[43,44] which supporting octahedral geometry. The electronic absorption spectrum of the Co(II) complex gives two bands at 18867 and 17857 cm^{-1} The bands observed are assigned to the transitions $^4T_{1g}$ (F)→$^4T_{1g}$ (P) and $^4T_{1g}$ (F)→$^4T_{1g}$ (F), respectively, suggesting an octahedral geometry around Co(II) ion.[45–49] The electronic absorption spectrum of the Ni(II) complex displays one band at 19607 cm^{-1}, which may be assigned to $^3A_{2g}$→$^3T_{1g}$ (P) transition which supporting distorted octahedral geometry.[45,46] The absorption spectrum of the Cu(II) chelate consists of one band at 19230 cm^{-1} which can be attributed to the $^2B_{1g}$→^2E_g transition with 10Dq 235 kj/mol with crystal field stabilization

Table 3. UV-vis. Spectra for **TXA** and its metal complexes.

Compound	λ_{max} (nm)	ν (cm^{-1})	Peak Assignment	ε ($M^{-1}cm^{-1}$) x 10^4	10Dq cm^{-1}	kJ/mol	CFSE	μ_{eff} (B.M)
TXA	295	33898	$\pi\rightarrow\pi^*$	0.425	–	–	–	–
	315	31746	$n\rightarrow\pi^*$	0.154				
(1)	290	34482	$\pi\rightarrow\pi^*$	0.421				
	320	31250	$n\rightarrow\pi^*$	0.153				
	460	21739	LMCT	0.006	18181	358	-573 + p	5.63
	550	18181	d-d transition	0.064				
(2)	292	34246	$\pi\rightarrow\pi^*$	0.423				
	325	30769	$n\rightarrow\pi^*$	0.154		226	−497 + 2p	5.11
	463	21598	LMCT	0.073	18867	214	−530 + 2p	
	530	18867	d-d transition	0.066	17857			
	560	17857	d-d transition	0.056				
(3)	290	34482	$\pi\rightarrow\pi^*$	0.424				
	320	31250	$n\rightarrow\pi^*$	0.155				
	475	21052	LMCT	0.074	19230	230	−276 + 3p	3.31
	520	19230	d-d transition	0.077				
(4)	293	34129	$\pi\rightarrow\pi^*$	0.420				
	325	30769	$n\rightarrow\pi^*$	0.156				
	450	22222	LMCT	0.073	19607	235	−141 + 4p	1.70
	510	19607	d-d transition	0.054				
(5)	291	40983	$\pi\rightarrow\pi^*$	0.461				
	325	36363	$n\rightarrow\pi^*$	0.159				
	445	22471	LMCT	0.078				

energy (CFSE) −141 + 4p octahedral Cu(II) structure.[46,47] Complex **(5)** was diamagnetic and indicates the geometry of the octahedral.

2.4. Optical Band Gap Energy (E_g)

The absorption bands in UV-vis spectra, which display an abrupt rise in ab-sorption known as the absorption edge, were used to determine E_g for our compounds. Eg has been determined from Tuac's equation to clarify the conductivity of the compounds.[50,51]

$$\alpha h\nu = \left(h\nu - E_g\right)^n \quad (1)$$

where, hν = energy of photon; n = $^1/_2$ and 2 for direct and indirect transition. α = absorption coefficient.

$$\alpha = 1/d\ln(1/T) \quad (2)$$

where, T = estimated transmittance and d = optical path length of the cuvette

Figure 1 shows a plot of $(\alpha h\nu)^2$ against h*ν*, with E_g produced by extrapolating the linear component of the curve to $(\alpha h\nu)^2 = 0$. The curve clearly shows that the direct values of E_g equal 4.28, 4.12, 4.10, 4.08, 4.11 and 4.13 eV for **TXA**, **(1)**, **(2)**, **(3)**, **(4)** and **(5)** respectively. The complexes' E_g estimates were lower than the **TXA**, which may attributable to electron migration towards metal ions.[52] In actuality, the low E_g value which may attributable to electron migration towards metal ions.[52] makes the molecule more electro conductive by allowing electrical transitions between the LUMO-HOMO energy states to occur more easily.[53,54]

2.5. ^{1}H-NMR Spectra

The combination of the integration and multiplicity pattern of protons has been utilized for assigning resonance in ^{1}H-NMR spectrum data for **TXA** and Zr(IV) compounds. Figure 2 and *Table S1* show the chemical shifts of the various proton types in the ^{1}H-NMR spectra of the **TXA** and Zr(IV) complex. ^{1}H-NMR spectrum of **TXA** showed δ(H) at 0.54 ppm (m, J = 2.16, H–C (3,4,6,7), 8H), δ(H): 0.76 (d, J = 3.09, H–C(1), 2H) corresponding to $-CH_2$ group of cyclohexane and corresponding to $-CH_2$ group of methylene. at δ(H) 2.04 ppm for -NH_2 amine group[55,56] The **TXA** spectrum's signal at δ:11.00 ppm can be attributed to the carboxylic (−COOH) proton.[57] The lack of the carboxylic proton (−COOH) in the complex spectrum, which **TXA** is coordinated through deprotonated carboxylate oxygen atoms.[58] The diamagnetic Zr(IV) complex's ^{1} H-NMR spectrum reveals a new signal at δ:3.82 ppm, which is assigned to water molecule abundance.[59] When spectra of **TXA** and its complex were compared, the complex spectrum shows all of the free **TXA** signals in addition to some changes from the ligand's binding to the metal.[60,61]

2.6. Mass Spectra

Mass spectrometry of our complexes (Figure S3) showed the molecular formulae of complexes **(1)**, **(2)**, **(3)**, **(4)** and **(5)** at 475 (81.25 %), 425 (21.20 %), 461 (79.36 %), 447 (39.19 %) and 473

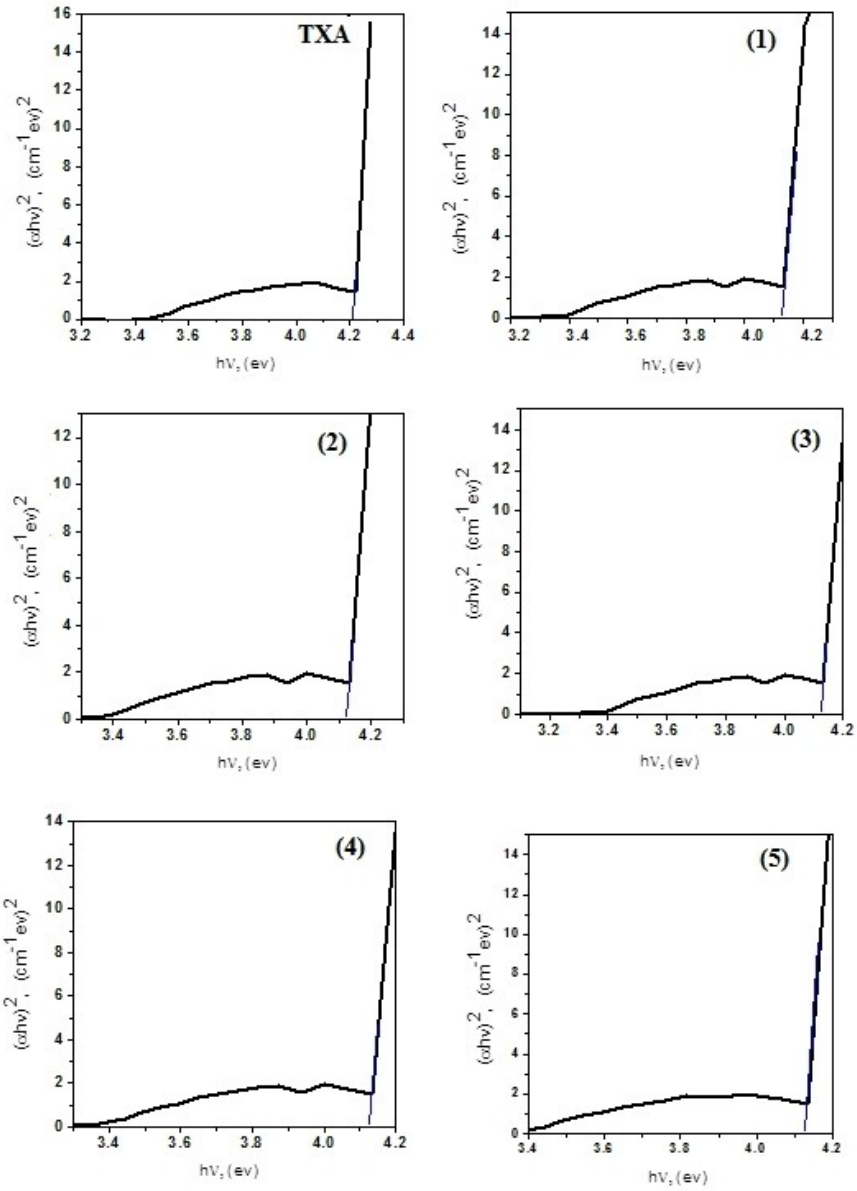

Figure 1. Allowed direct band gaps of **TXA** and its complexes.

(78.52%), respectively, the highest mass peak m/z = amu. These data were very much in line with the formulae weight of the complexes. Scheme 3 manifest the fragmentation manner of complex **(1)** as representative case. Where at m/z = 475 (81.25%) allocated to the molecular ion peak [a] losses H_2O to produce [b] at m/z = 457 (79.20%) and losses $2H_2O$ to produce [c] at m/z = 439 (63.18%). The peak molecular ion [a] losses $Cl.H_2O$ at m/z = 421 (59.21%) to give [d] and losses $Cl.2H_2O$ to produce [e] at m/z = 403 (44.97%) in order to produce fragment [f] at m/z = 459 (98.88%).

2.7. Thermal Analysis Sudies (TG and DTG)

A temperature range of 1000 °C to room temperature (*Figure S4*). The TG results exhibit a strong correlation with the proposed formulas derived from the microanalysis data (Table 1), temperature ranges, percentage, T_{max} and lost species of the solid complexes were given in Table 4. The **TXA**'**s** TG curve indicated a single-step disintegration at T_{max} 284 °C with an estimated mass loss of (100.00%) with the removal of $4\,C_2H_2 + 2H_2O + NH_3$. Complex **(1)** thermally stable up to 55 °C and the decay originated from 55 to 900 °C three steps. The first decay step within the 55 to 124 °C range T_{max} 116 °C corresponds to the loss of lattice water molecules ($2H_2O$) with a weight loss 7.50% (calc. 7.56%). The second step at T_{max} 263 °C assigned to loss of $4\,C_2H_4 + 2H_2O$ with weight loss 29.90% (calcd. 29.42%).

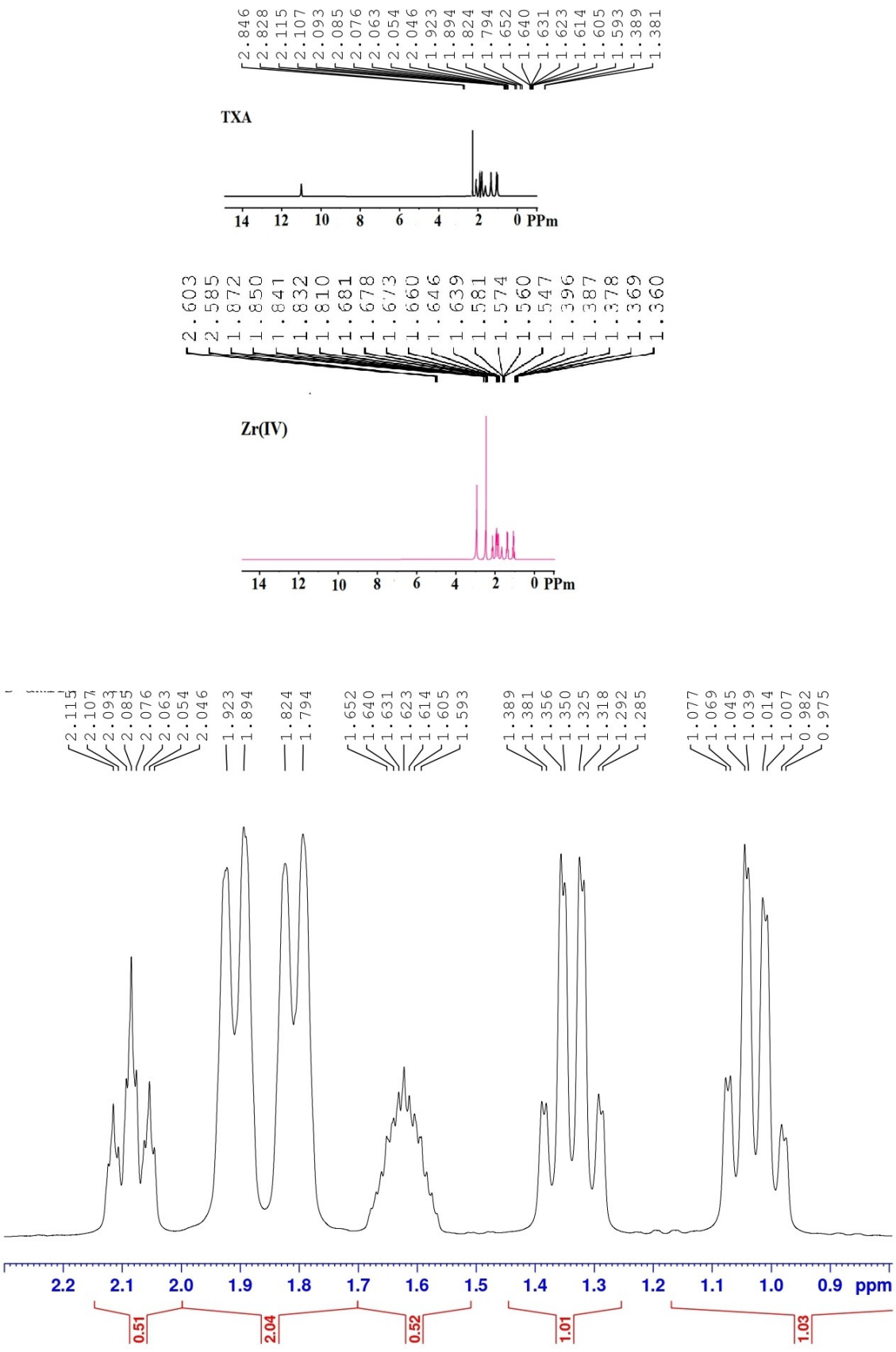

Figure 2. [1] H-NMR spectra for ***TXA*** and Zr(IV) complex.

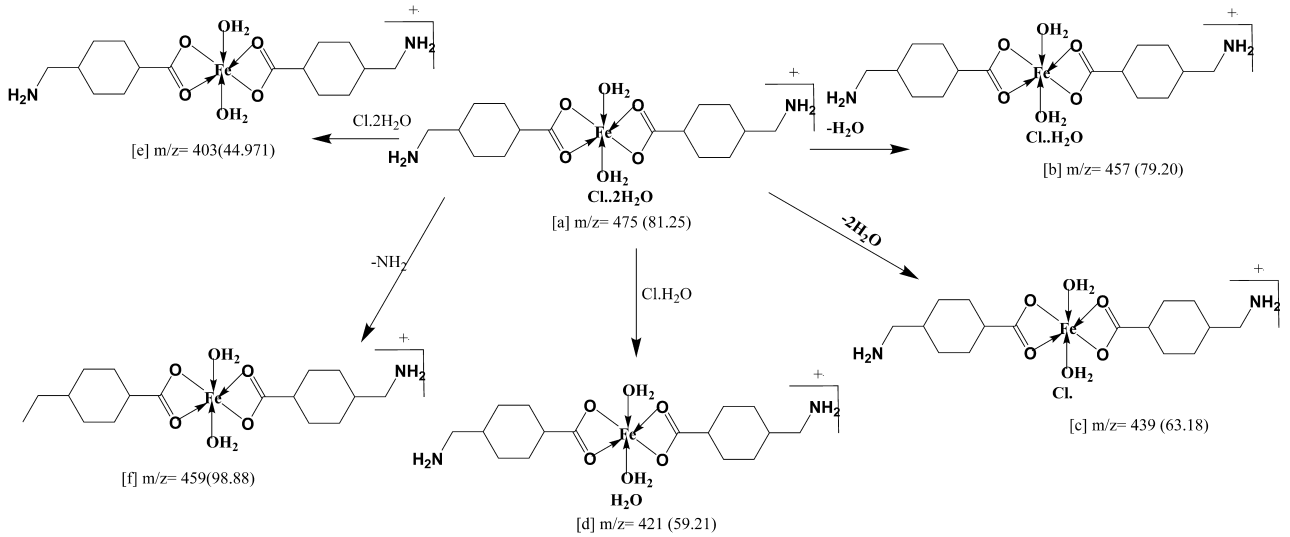

Scheme 3. Fragmentation pattern of complex (1).

Table 4. Maximum temperature T_{max}(°C) and weight loss values of the decomposition stages for **TXA** and its metal complexes.

Compounds	Decomposition	Temperature range (°C)	T_{max}(°C)	Weight loss (%)		Lost species
				Calc.	Found	
TXA	First step	230–380	284	100.00	100.00	$4\,C_2H_2 + 2H_2O + NH_3$
	Total loss			100.00	100.00	
(1)	First step	55–124	116	7.56	7.50	$2H_2O$
	Second step	124–278	263	29.42	29.90	$4\,C_2H_2 + 2H_2O$
	Third step	278–900	403, 866	51.29	51.60	$4\,C_2H_2 + HCl + 2H_2O + NH_3 + NO_2 + 2H_2$
	Total loss			88.27	89.00	
	Residue			11.73	11.00	Fe
(2)	First step	60–120	65	4.24	4.20	H_2O
	Second step	120–309	254	20.68	20.22	$2\,C_2H_2 + 2H_2O$
	Third step	309–927	405, 462, 831	51.83	52.48	$4\,C_2H_4 + H_2O + 2NH_3 + 2CO$
	Total loss			76.75	76.90	
	Residue			23.25	23.10	$CoO + 2\,C$
(3)	First step	55–120	98	11.71	11.70	$3H_2O$
	Second step	120–569	238, 326	57.25	57.24	$6\,C_2H_2 + 6H_2O$
	Third step	569–904	875	13.11	13.49	$C_2H_2 + 2NH_3$
	Total loss			82.07	82.43	
	Residue			17.93	17.57	$Ni + 2\,C$
(4)	First step	58–125	85	8.03	8.00	$2H_2O$
	Second step	125–473	226, 429	49.11	49.00	$5\,C_2H_2 + 5H_2O$
	Third step	473–900	493, 875	25.10	25.39	$3\,C_2H_2 + 2NH_3$
	Total loss			82.25	82.39	
	Residue			17.75	17.61	CuO
(5)	First step	55–123	75	7.60	7.58	$2H_2O$
	Second step	123–654	259, 407	57.42	57.40	$7\,C_2H_2 + 5H_2O$
	Third step	654–900	892	13.19	13.38	$2NH_3 + CO$
	Total loss			78.21	78.36	
	Residue			21.79	21.64	$Zr + C$

The third step with T_{max} 403, 866 °C matched to 4 C_2H_2 + HCl + 2H_2O + NH_3 + NO_2 + 2H_2 with weight loss of 51.60% (calc.51.29%) leaving Fe as a residue. TG of complex **(2)** proceeded throughout the temperature range 60 °C to 927 °C with three stages. The first step at T_{max} 65 °C corresponding to lack of H_2O (weight loss: 4.20%, calc. 4.24%). The subsequent stages demonstrated the demise of 2 C_2H_2 + 2H_2O (found:72.70%, calc. 72.51%) and 4 C_2H_4 + 2NH_3 + H_2O + 2CO leaving a CoO + 2 C as a final product. The compound **(3)** underwent three declining phases in its thermal disintegration within the temperature range of 55 °C to 904 °C at T_{max} (98, 238, 326 and 875 °C) with mass loss (found 11.70%, calc.11.71%), (found: 57.24%, calc. 57.25%) and (found: 13.49%, calc. 13.11%) matching to the loss of 3H_2O, 6 C_2H_2 + 6H_2O and C_2H_2 + 2NH_3 leaving Ni + 2 C as a residue. Moreover, Complexes **(4)** and **(5)**, broke down into three parts. The initial stage verified the lattice water loss at T_{max} 85 and 75 °C. The second step corresponding to the loss of 5 C_2H_2 + 5H_2O and 7 C_2H_2 + 5H_2O finally the third step assigned to the loss of 3 C_2H_2 + 2NH_3 and 2NH_3 + CO leaving CuO and Zr + C as thermal decomposition. The nature of the residue was identified using infrared spectra (Figure S5) and XRD analysis (Figure S6), the values of peaks characteristic for the metal oxides were found.

2.8. Differential Thermal Analysis (DTA)

The DTA nitrogen thermogram of **TXA** (Figure 3*)*, with metal complexes under investigation reveals various phases in accordance with the prior DTA assessment. The chemical changes that occur when water, anion, and ligand molecules are removed are seen as exo- or endothermic peaks in the DTA curves. At 284 °C the **TXA** offers one peak as endothermic peak with activation energy −26.23uv. The complex **(1)** manifested several peaks (endothermic and exothermic) of −3.81, −4.51, −1.73, −0.42, 7.01, −0.21 and-1.44 uV at 124, 264, 317, 368, 401, 498 and 870 °C, respectively. Diverse endothermic and exothermic peaks at 221, 260, 406, 464 and 767 °C with activation energies for complex **(2)** −2.61, −2.85, −5.40, 7.51 and −0.75 uV. DTA curve of complex **(3)** manifest six peaks at 76 °C, 107, 317, 342, 763 and 881 °C with activation energies −3.5, −14.07, 9.91, −3.42, −1.46 and −59.93uV. The complex **(4)** has several peaks (endothermic and exothermic) of −17.48, 33.75, 1.87 and 49.49 uV activation energies at different temperatures of 87, 226, 461 and 493 °C respectively. The absence of hydration of water molecules was matched by the first endothermic peak at 87 °C, which had an activation energy of −17.48 uV. The final exothermic peaks at 226, 461, and 493 °C were matched by the abstraction of coordinated water and **TXA** molecules, which had activation values of 33.75, 1.87, and 49.49 uV. Diverse endothermic peaks manifestation at Diverse temperature 79, 260, 372, 769 and 895 °C with activation energies −3.38, 6.74, −0.93, −1.43 and −11.67 uV for complex **(5).**

2.9. Calculations of Activation Thermodynamic Parameters

Using the coats-Redfern[62] and Horowitz-Metzger models,[63] kinetic thermodynamic characteristics of the thermal degradation process, such as (E_a), (ΔS*), (ΔH*), and (ΔG*), were visually analyzed.

The data were summarized in Table 5 and figure S7. The E_a values for **TXA** and its complexes found in the range of 12.21–130.17 kJ/mol according to Coats-Redfern model and in the range 12.67–136.63 kJ/mol according to Horowitz-Metzger model for the **TXA** ligand and its ligand complexes. The complexes' thermal stability is shown in the high E_a values. All complexes had negative values for ΔS*, indicating their stability.[32] The positive sign of ΔG* for the complexes under investigation indicated that the free energy of the final residue was greater than that of the starting molecule, indicating that all stages of the decomposition process were not spontaneous. The positive data of ΔH* suggest that the decay process is endothermic.[35] For each complex, the values of ΔG* climbed dramatically as it decomposed more. This can be explained by showing that values of ΔH* are overridden when TΔS* values are greatly increased from one step to the next.[64]

2.10. Antimicrobial Activity

2.10.1. Bactericidal Effect

The studied ligand (TXA) and its new prepared metal-complexes were evaluated for eventual antibacterial effect against *B. megaterium*, *E. coli* and *X. campestris* (Table 6). The obtained results showed that all tested compounds had promising antibacterial effects against all tested bacteria especially at the higher tested dose. In particular, complexes **(1)**, **(2)** and **(3)** showed the highest substantial affect against *X. campestris* was obtained at 4000 ppm. Regarding *B. megaterium* and *E. coli.* The highest affect was observed in the case of complex **(3)** and complex **(1)**, respectively at 4000 ppm. On the other side, complex **(1)** and **(4) at** 500 ppm showed the lowest effect against *X. campestris* (Table 6). However, none of the tested compounds showed any effect at 500 ppm against *B. megaterium* and *E. coli.*

2.10.2. Fungicidal Effect

TXA and its complexes were evaluated for fungicidal effect against *F. oxysporum*, *M. fructicola* and *P. italicum* (Table 7*)*. Results were demonstrated as diameter of inhibition zones (cm). All examined substances clarified antifungal effect in a dose dependent manner. Most of tested compounds demonstrated significant higher effect against the three tested fungi. On the other side, complex **(3)** at 500 ppm demonstrated lowest effect against *M. fructicola.*

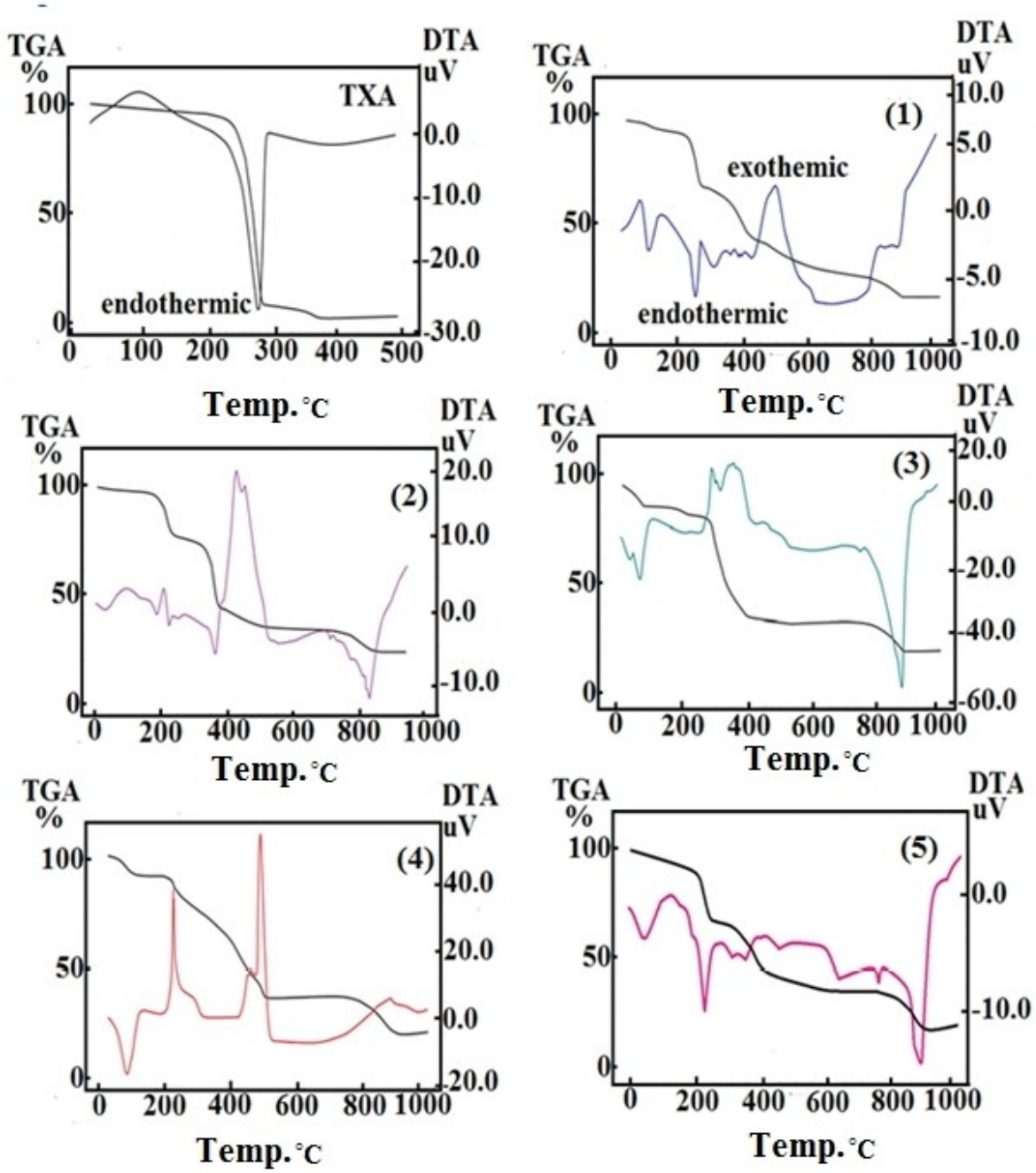

Figure 3. DTA diagrams for **TXA** and its metal complexes.

2.10.3. Mode of Action

The antibacterial impact that was discovered in the investigated ligand and metal-complexes may have something to do with the **TXA** ligand's chemical structure and the metal ions' toxic properties.[65] In addition, the cell permeability theory of the microbial cell wall can clarify the obtained antimicrobial activity of the metal chelate.[65,66] In instance, orbital overlap with the parent ligand and partial charge sharing with the its donor groups may minimize the polarity of metal ions.[67] On the other side, the chelation process can promote the delocalization of electrons on the chelate ring, and can enhance the lipophilicity of the central ions allowing the new complexes to easily penetrate into the microbial cells.[68]

2.11. Phytotoxicity

The obtained results of phytotoxicity (Table 8) revealed that, the three compounds **TXA**, **(4)** and **(5)** showed complete phytotoxic effect against the three tested plants seeds at all concentrations. On the other hand, **(1)**, **(2)** and **(3)** showed

Table 5. Thermal behavior and kinetic parameters for **TXA** and its metal complexes.

Compounds	Decomposition Range (K)	T_s (K)	Method	Parameter					R [a]	SD [b]
				E_a (kJ/mol)	A (s^{-1})	ΔS* (kJ/mol·K)	ΔH* (kJ/mol)	ΔG* (kJ/mol)		
TXA	478–571	557	CR	71.38	3.10×10^{4}	−0.1641	66.75	158.16	0.981	0.219
			HM	78.72	1.22×10^{5}	−0.1527	74.09	159.15	0.972	0.264
(1)	313–683	529	CR	25.17	0.9172	−0.2478	21.93	118.34	0.989	0.109
			HM	29.36	3.398×10^{1}	−0.1278	26.12	110.85	0.981	0.145
	437–551	536	CR	43.91	2.64×10^{1}	−0.2225	39.45	158.74	0.980	0.160
			HM	52.78	5.11×10^{2}	−0.1979	48.33	154.41	0.968	0.200
(2)	459–582	527	CR	35.27	9.42×10^{-5}	−0.2501	30.89	153.92	0.984	0.156
			HM	71.38	2.6740	−0.2414	26.67	162.71	0.966	0.229
	581–701	679	CR	130.17	2.19×10^{8}	−0.0910	124.53	186.39	0.975	0.181
			HM	163.36	2.61×10^{10}	−0.0523	157.72	188.01	0.971	0.198
(3)	324–400	371	CR	16.16	5.81×10^{-4}	−0.2703	13.08	113.39	0.990	0.071
			HM	18.87	1.2423	−0.2449	15.78	106.65	0.994	0.052
	434–541	511	CR	63.92	1.21×10^{4}	−0.1711	59.67	147.14	0.992	0.101
			HM	83.06	1.96×10^{6}	−0.1289	78.81	144.68	0.989	0.117
(4)	303–399	355	CR	13.83	2.22×10^{-4}	−0.2779	10.88	109.57	0.997	0.062
			HM	14.95	3.75×10^{-5}	−0.2545	12.00	102.34	0.989	0.117
	439–585	500	CR	21.43	3.11×10^{-4}	−0.2780	17.27	156.29	0.991	0.105
			HM	17.27	8.79×10^{-4}	−0.2694	13.11	147.82	0.969	0.200
	746–840	766	CR	91.22	1.04×10^{3}	−0.1949	84.85	234.17	0.994	0.089
			HM	87.71	2.85×10^{3}	−0.1865	81.34	224.26	0.992	0.112
(5)	306–446	346	CR	12.21	1.55×10^{-4}	−0.2807	9.33	106.48	0.998	0.033
			HM	12.67	1.72×10^{-5}	−0.2607	9.79	100.00	0.993	0.070
	446-555	532	CR	25.47	1.11×10^{-5}	−0.2679	21.54	164.07	0.990	0.106
			HM	28.07	1.1300	−0.2487	23.64	155.95	0.976	0.167

a = correlation coefficients of the Arrhenius plots and b = standard deviation.

Table 6. Antibacterial activity of **TXA** and its metal complexes.

		Diameter of inhibition zones (cm)						
	μg/ml	**TXA**	**(1)**	**(2)**	**(3)**	**(4)**	**(5)**	**Tetracycline**
B. megaterium	4000	0.9 ± 0.02b	0.7 ± 0.04b	1.0 ± 0.1b	1.6 ± 0.2a	1.0 ± 0.1b	0.9 ± 0.02b	0,0
	1000	0.6 ± 0.01c	0.5 ± 0.03c	0.8 ± 0.02b	0.5 ± 0.04c	1.0 ± 0.3b	0.6 ± 0.01c	0,0
	500	0.0 ± 0.0d	0.0 ± 0.0d	0.0 ± 0.0d	0.0 ± 0.0d	0.0 ± 0.0d	0.0 ± 0.0d	0,0
E. coli	4000	1.1 ± 0.3ab	1.5 ± 0.3a	1.1 ± 0.2ab	0.7 ± 0.05b	0.8 ± 0.01b	1.1 ± 0.3ab	0,0
	1000	0.7 ± 0.02b	1.2 ± 0.4ab	0.6 ± 0.05b	0.3 ± 0.04c	0.4 ± 0.05c	0.7 ± 0.02b	0,0
	500	0.0 ± 0.0d	0.0 ± 0.0d	0.0 ± 0.0d	0.0 ± 0.0d	0.0 ± 0.0d	0.0 ± 0.0d	0,0
X. campestris	4000	1.6 ± 0.1b	2.3 ± 0.4a	2.5 ± 0.4a	2.5 ± 0.2a	1.5 ± 0.4b	1.6 ± 0.1b	0,0
	1000	1.0 ± 0.02bc	1.2 ± 0.3bc	2.0 ± 0.5ab	1.5 ± 0.4b	1.0 ± 0.2bc	1.0 ± 0.02bc	0,0
	500	0.6 ± 0.01c	0.3 ± 0.01c	1.3 ± 0.2b	1.0 ± 0.1bc	0.4 ± 0.02c	0.6 ± 0.01c	0,0

Values were recorded as the mean of three replicates of diameter of inhibition zones in cm (± SDs). Values followed by different letters in each row are significantly different according to *Tukey* B test at $P < 0.05$. Tetracycline: the positive control at 1600 μg/mL.

varied effects against the three tested plants ranged from higher (in case of 4000 ppm) to moderate effect (in case of 1000 and 500 ppm). The complexes **(2)** and **(3)** at 500 ppm showed the higher germination index in case of *L. sativum*. Whereas, the same compounds showed moderate and very low germination index against *L. sativa* and *S. lycopersicum*, respectively. These results indicated the possibility of these studied compounds to be used in the control of harmful weeds.

3. Materials and Methods

3.1. Materials

The analytical reagent grade (AR) and purest possible whole compounds were employed. Sigma and Aldrich chemicals provided the **TXA**, potassium hydroxide, ferric chloride, cobalt chloride hexahydrate, nickel chloride dihydrate, copper chloride dihydrate, zirconyl chloride heptahydrate, potassium dichromate, concentrated sulfuric acid 98%, commercial grade concentrated nitric acid

Table 7. Antifungal activity of **TXA** and its metal complexes.

		Diameter of inhibition zones (cm)					
	µg/ml	**TXA**	**(1)**	**(2)**	**(3)**	**(4)**	**(5)**
F. oxysporum	4000	3.8 ± 0.8ab	4.5 ± 1.0a	3.8 ± 1.5ab	4.5 ± 0.8a	4.5 ± 0.8a	3.8 ± 1.2ab
	1000	3.5 ± 0.9b	4.0 ± 0.9ab	3.0 ± 1.1bc	3.8 ± 1.7ab	3.9 ± 0.5ab	3.5 ± 1.2b
	500	2.0 ± 0.5c	3.0 ± 0.7bc	2.2 ± 1.2c	3.0 ± 1.1bc	3.0 ± 1.5bc	2.0 ± 0.9c
M. fructicola	4000	3.5 ± 1.0b	4.5 ± 0.6a	4.5 ± 1.1a	3.5 ± 1.0b	3.5 ± 1.1b	3.5 ± 1.3b
	1000	3.0 ± 1.2bc	4.32 ± 1.2a	4.0 ± 1.9ab	3.0 ± 1.1bc	3.0 ± 1.2bc	3.0 ± 0.9bc
	500	1.5 ± 0.4cd	3.9 ± 1.4ab	3.0 ± 0.8	1.3 ± 0.5cd	1.8 ± 0.5cd	1.5 ± 0.4cd
P. italicum	4000	4.5 ± 0.8a	4.5 ± 1.6a	4.0 ± 1.7ab	4.5 ± 1.3a	4.5 ± 1.4a	4.5 ± 2.0a
	1000	4.0 ± 1.4ab	3.9 ± 0.9ab	3.5 ± 0.6b	4.0 ± 1.7ab	4.3 ± 0.9a	4.0 ± 1.5ab
	500	3.0 ± 1.0bc	3.0 ± 0.6bc	2.9 ± 1.3bc	3.9 ± 0.6ab	3.9 ± 0.8ab	3.0 ± 1.3bc

Values were recorded as the mean of three replicates of diameter of inhibition zones in cm (± SDs). Values followed by different letters in each row are significantly different according to *Tukey* B test at $P < 0.05$.

Table 8. Phytotoxicity of **TXA** and its metal complexes.

		Germination Index (%)		
	µg/ml	*L. sativum*	*L. sativa*	*S. lycopersicum*
TXA	4000	0,0 ± 0,0e	0,0 ± 0,0d	0,0 ± 0,0d
	1000	0,0 ± 0,0e	0,0 ± 0,0d	0,0 ± 0,0d
	500	0,0 ± 0,0e	0,0 ± 0,0d	0,0 ± 0,0d
(1)	4000	0,0 ± 0,0e	0,0 ± 0,0d	0,0 ± 0,0d
	1000	0,6 ± 0,2d	2,1 ± 0,6bc	0,2 ± 0,1c
	500	1,7 ± 0,4c	4,0 ± 0,8b	1,1 ± 0,1b
(2)	4000	0,1 ± 0,1d	0,0 ± 0,0d	0,0 ± 0,0d
	1000	4,4 ± 1,1c	0,7 ± 0,3c	0,0 ± 0,0d
	500	16,3 ± 1,8b	5,6 ± 0,6b	0,9 ± 0,3b
(3)	4000	0,0 ± 0,0e	0,0 ± 0,0d	0,0 ± 0,0d
	1000	2,2 ± 0,6c	0,4 ± 0,2c	0,0 ± 0,0d
	500	13,9 ± 4,2b	4,3 ± 0,2b	0,6 ± 0,1c
(4)	4000	0,0 ± 0,0e	0,0 ± 0,0d	0,0 ± 0,0d
	1000	0,0 ± 0,0e	0,0 ± 0,0d	0,0 ± 0,0d
	500	0,0 ± 0,0e	0,0 ± 0,0d	0,0 ± 0,0d
(5)	4000	0,0 ± 0,0e	0,0 ± 0,0d	0,0 ± 0,0d
	1000	0,0 ± 0,0e	0,0 ± 0,0d	0,0 ± 0,0d
	500	0,0 ± 0,0e	0,0 ± 0,0d	0,0 ± 0,0d
Control H_2O		100,0 ± 0,0a	100,0 ± 0,0a	100,0 ± 0,0a

Values were recorded as the mean of three replicates (± SDs). Values followed by different letters in each vertical column are significantly different according to *Tukey* B test at $P < 0.05$.

69%, hydrogen peroxide 20%, disodium salt EDTA, ammonium chloride, ammonium hydroxide, variamine blue, eriochrome black T, gallein (Pyrogallolphthalein), silver nitrate, absolute ethyl alcohol, Dimethyl sulfoxide (DMSO), and dimethylformamide (DMF), were supplied, respectively. All preparations typically used distilled water. Every piece of glassware was soaked in a chromic combination (potassium dichromate + concentrated sulfuric acid) for an entire night. It was then completely rinsed with bidistilled water and dried at 100 °C in an oven.

3.2. Synthesis of Metal Complexes

The Reddish brown $[Fe(\mathbf{TXA})_2(H_2O)_2]Cl.2H_2O$ solid complex **(1)** was created by mixing 2 mmol (0.31442 g) of **TXA** with 1 mmol (0.1622 g) of $FeCl_3$ in 20 mL of ethanol and 2 mmol (0.110 g) of KOH in 40 mL of pure ethanol. The mixture was refluxed for four hours and the formed precipitate, filtered off and vacuum-dried over anhydrous calcium chloride. The Violet, Pale green, dark green, and Light white complexes $[Co(\mathbf{TXA})_2(H_2O)_2].H_2O$ **(2)**, $[Ni(\mathbf{TXA})_2(H_2O)_2].3H_2O$ **(3)**, $[Cu(\mathbf{TXA})_2(H_2O)_2].2H_2O$ **(4)** and $[ZrO(\mathbf{TXA})_2(H_2O)].2H_2O$ **(5)** were created in the same way as previously mentioned, employing ethanol as a solvent and a 1:2:2 (M:TXA:KOH) molar ratio to create cobalt chloride hexahydrate, nickel chloride dihydrate, copper chloride dihydrate, and zirconyl chloride octahydrate, respectively. The yields varied from 79.21 to 88.63 percent.

3.3. Instruments

A Perkin Elmer 2400 CHN elemental analyzer was used to carry out the elemental studies. Three analytical techniques – complexometric titration, thermogravimetry, and atomic absorption – were utilized for estimating the M% content. The metal complexes were broken down using a digestion process in order to prepare for complexometric titration. To initiate the digestion process, two milliliters of nitric acid and one milliliter of hydrogen peroxide were added to a beaker containing a precisely weighed metal complex. Next, the beaker was heated to a maximum temperature of 85 °C on a hot plate. It was then covered with an elevated watch glass, allowed to cool, and then diluted to 25 mL using bi-distilled water in a volumetric flask. By converting the solid goods into metal or metal oxide and applying the atomic absorption method, the fraction of metal ions was ascertained gravimetrically.[30] The direct method of atomic absorption analysis was used to measure the total metal content at the corresponding wavelength. For every metal, multiple reference standard solutions were made at a certain concentration. For this, a PYE-UNICAM SP 1900 spectrum equipped with the appropriate lamp was utilized. The FT-IR spectra of KBr discs were obtained within the 4000–400 cm^{-1} range using Spectrophotometer FT-IR 460 PLUS. DMSO-d6 was used as the solvent to record ^{1}H-NMR spectra on a Varian Mercury VX-300 NMR Spectrometer. Using a TGA-50H Shimadzu, TG-DTG measurements were performed in a N_2 environment between room temperature and 1000 °C. The mass of the sample was precisely weighed out in

an aluminum crucible. The UV-3101PC Shimadzu was used to analyze the electronic spectra. The solutions in DMSO-d6 were used to record the absorption spectra. Using a Gouy balance Hg[Co-(CSN)$_4$] used as the calibrant, the room temperature magnetic susceptibilities of the powdered materials were examined using a Sherwood scientific magnetic balance. Melting points were measured using a Buchi device. Mass spectra in the range 0–1090 registered on GCMS-QP-1000EX Shimadzu (ESI-70ev). Using CONSORT K410, the molar conductance of 1×10^{-3} M solutions of **TXA** and their complexes in DMF was determined. Every measurement was done using freshly made solutions at room temperature.

3.4. Antibacterial Activity Assay

Tested bacteria. The tested bacterial strains were conserved as pure cultures in the collection of the School of Agricultural, Forestry, Food and Environmental Sciences (SAFE), University of Basilicata, Potenza, Italy.

Bactericidal assay. The eventual antibacterial activity assay has been carried out following disc diffusion method.[69] Bacterial suspensions at 10^8 colony form units (CFU) adjusted using spectrophotometer (DAS s.r.l., Rome, Italy) were prepared in sterile Millipore H_2O and added into soft agar (0.7%). Four mL of each bacterial suspension were poured into Petri dishes (Ø 90 mm). Blank Discs (Ø 6 mm) (OXOID, Milan, Italy) were then placed on KB Petri and treated with 15 μL of each tested compound at concentrations 4000, 1000 and 500 μg/mL. Tetracycline (1600 μg/mL) was utilized as control. All plates were incubated at 37 °C for 24 h. The antimicrobial effect was determined by measuring the diameter of inhibition zones (cm). The experiment was carried out in triplicate and standard deviations (±SDs) were measured.

3.5. Antifungal Activity Assay

Tested fungi. The tested phytopathogenic fungi, were cultured on potato dextrose agar (PDA) and were previously identified using morphological and molecular methods. All tested fungi were stored at 4 °C as pure cultures in the mycotheca of SAFE, University of Basilicata, Potenza, Italy.

Fungicidal assay. The eventual antifungal effect of the tested compounds was evaluated following agar well diffusion technique[70] at concentrations 4000, 1000 and 500 μg/ml. Every Petri dish (Ø 90 mm) was inoculated with a fungal disk (0.5 cm), from 96 h fresh culture. A hole with a diameter of 4 mm is punched aseptically with a sterile cork-borer and a volume of 15 μL of each tested concentration were added. All plates were incubated at 24 °C for 96 h and the antifungal effect was estimated by measuring the diameter of inhibition zones (cm). The experiment was carried out in triplicate and standard deviations (±SDs) were measured.

3.6. Phytotoxicity Assay

A bioassay based on SG-RE was carried out to evaluate the possible phytotoxic effect of **TXA** and its metal complexes on *L. sativum*, *L. sativa* and *S. lycopersicum* seeds.[71] The seeds were pre-sterilized in 3% H_2O_2 solution for 1 min and then were rinsed twice with deionized sterile water (dH_2O), then were placed either in dH_2O (negative control) or tested compounds at concentrations 4000, 1000 and 500 μg/ml and were shaken gently for 2 hrs. Ten seeds of each species were separately placed on top of the filter paper (Whatman No.1) in each Petri dish (Ø 90 mm) and filled with 2 ml of dH_2O or different treatments and sealed with parafilm. All petri dishes were incubated in a growth chamber at 28±2 °C with 60% relative humidity in darkness for 4–6 days. The number of germinated seeds was counted and the radical length was measured in cm. The experiment was conducted in triplicate and the germination index (GI) was calculated using the formula:

$$\text{G.I. } \% = [(\text{SGt x REt})/(\text{SGc x REc})] \text{ x } 100 \quad (3)$$

where: GI: germination index; SGt: average number of germinated treated seeds; REt: average radical elongation for treated seeds; SGc: average number of germinated seeds for negative control; REc: average radical elongation for negative control. Data are expressed as mean values (±SDs). Data were analyzed using SPSS statistical program with Tukey test at $P < 0.05$.

4. Conclusions

We synthesized and characterized novel compounds containing **TXA**, including Fe(III), Co(II), Cu(II), Ni(II), and Zr(IV). **TXA** functioned as a bidentate ligand through two oxygen atoms, and the octahedral geometry was seen in each compound. Except of the Fe(III) complex, none of the complexes were electrolytes. The existence of organized water has been established by TG and FT-IR tests. Research on magnetic susceptibility indicates that Fe(III) and Co(II) metal complexes persist in high-spin states. DTA analysis highlights the chemical changes caused by the removal of ligand, anion, and water molecules as exo- or endothermic peaks. The activation kinetic factors were determined at $n = 1$ and $n \neq 1$.

Supplementary Materials

The following supporting information can be downloaded at: www.mdpi.com/xxx/s1. Figure S1. Infrared spectra for TXA and its metal complexes; Figure S2. Electronic absorption spectra for TXA and its metal complexes; Figure S3: Mass spectra diagrams for TXA metal complexes; Figure S4. TG and DTG diagrams for TXA and its metal complexes; Figure S5. Infrared spectra of CoO and Cuo; Figure S6: XRD of CoO and CuO; Figure S7.The diagrams of kinetic parameters of TXA ligand and its metal complexes; Table S1. ^{1}H-NMR signals of the TXA and Zr(IV) complex.

Funding

This research received no external funding.

Institutional Review Board Statement

Not applicable.

Informed Consent Statement

Not applicable.

Author Contributions

Conceptualization, A. Mohamed and S. Sadeek; Formal analysis, A. Mohamed, N. Rashid and H.S. Elshafie; Investigation, S. Sadeek, N. Rashid and I. Camele; Supervision, S. Sadeek and I. Camele; Validation, A. Mohamed, S. Sadeek, H.S. Elshafie and I. Camele; Writing – original draft, A. Mohamed, H.S. Elshafie and I. Camele; Writing – review & editing, S. Sadeek and I. Camele.

Conflict of Interests

The authors declare no conflict of interest.

Data Availability Statement

The data that support the findings of this study are available from the corresponding author upon reasonable request.

Keywords: Tranexamic acid, metal complexes, antimicrobial activity · phytotoxicity · chelation theory · phytopathogens

[1] M. Hanif, Z. H. Chohan, *Spectrochim. Acta Part A* **2013**, *104*, 468–476.
[2] B. Lippert, *Coord. Chem. Rev.* **2000**, *487*, 200–202.
[3] N. Goswami, D. M. Eichhorn, *Inorg. Chim. Acta.* **2000**, *303*, 271–276.
[4] F. Dimiza, A. N. Papadopoulos, V. Tangoulis, V. Psycharis, C.P Raptopoulou, D. P, Kessissoglou, G. Psomas, *J. Inorg. Biochem.* **2012**, *107*, 54–64.
[5] E. Ortmann, M. W. Besser, A. A. Klein, *Br. J. Anaesth.* **2013**, *111*, 549–563.
[6] M. A. Longo, B. T. Cavalheiro, G. R. de Oliveira Filho, *J. Clin. Anesth.* **2018**, *48*, 32–38.
[7] Z. Dai, H. Chu, S. Wang, Y. Liang, *J. Clin. Anesth.* **2018**, *44*, 23–31.
[8] D. A. Henry, P. A. Carless, A. J. Moxey, D. O'Connell, B. J. Stokes, D. A. Fergusson, K. Ker, *Cochrane Database Syst. Rev.* **2011**, *19*.
[9] R. Karaman, H. Ghareeb, K. K. Dajani, L. Scrano, H. Hallak, H. H. Abu-Lafi, G. Mecca, S. A. Bufo, *J. Comput.-Aided Mol. Des.* **2013**, *27*, 615–635.
[10] A. S. Lukes, P. A. Kouides, K. A. Moore, *Women's Health* **2011**, *7*(2), 151–158.
[11] A. S. Lukes, K. A. Moore, K. N. Muse, J. K. Gersten, B. R. Hecht, M. Edlund, H. E. Richter, S. E. Eder, G. R. Attia, D. L. Patrick, A. Rubin, G. A. Shangold, *Obstet. Gynecol.* **2010**, *116*(4), 865–875.
[12] E'. Ortmann, M. W. Besser, A. A. Klein, *Br. J. Anaesth.* **2013**, *111*, 549–563.
[13] J. D. Jennings, M. K. Solarz, C. Haydel, *Orthop. Clin. North Am.* **2016**, *47*, 137–143.
[14] K. Ker, D. Prieto-Merino, I. Roberts, *Br. J. Surg.* **2013**, *100*, 1271–1279.
[15] L. D. Pacheco, G. R. Saade, M. M. Costantine, S. L. Clark, G. D. Hankins, *Am. J. Obstet. Gynecol.* **2016**, *214*, 340–344.
[16] S. Sigaut, B. Tremey, A. Ouattara, R. Couturier, C. Taberlet, S. Grassin-Delyle, J. F. Dreyfus, S. Schlumberger, M. Fischler, *Anesthesiology* **2014**, *120*, 590–600.
[17] P. S. Myles, J. A. Smith, A. Forbes, B. Silbert, M. Jayarajah, T. Painter, D. J. Cooper, S. Marasco, J. McNeil, J. S. Bussieres, S. McGuinness, K. Byrne, M. T. Chan, G. Landoni, S. Wallace, *N. Engl. J. Med.* **2017**, *376*, 136–148.
[18] I. Roberts, H. Shakur, A. Afolabi, K. Brohi, T. Coats, Y. Dewan, S. Gando, G. Guyatt, B. J. Hunt, C. Morales, P. D. Perel, Prieto-Merino, T. Woolley, *Lancet.* **2011**, *377*, 1101–1096.
[19] A. Turki, W. Michael, *Int. J. Neurol.* **2011**, *2011*, 203579. doi:10.4061/2011/203579.
[20] W. Sufan, S. Hangyan, W. Hua, Y. Sheng, G. Jincai, S. Yi, P. Lei, *Aesthet Plast. Surg.* **2012**, *36*, 964–970.
[21] A. A. Helaly, A. A. El-Bindary, S. A. Elsayed, *Int. Jo. Liq.* **2023**, *389*, 122831.
[22] M. A. El-Bindary, A. A. El-Bindary, *Appl. Organomet. Chem.* **2022**, *36*, e6576.
[23] P. W. Hsieh, W. Y. Chen, A. Aljuffali, C. C. Chen, J. Y. Fang, *Curr. Med. Chem.* **2013**, *20*, 4080–4092.
[24] J. Song, W. Duan, Y. Chen, X. Liu, *Chinese J. Struc. Chem.* **2022**, *41*, 2205037–2205047.
[25] W. J. Geary, *Coord. Chem. Rev.* **1971**, *7*, 81–122.
[26] G. N. Rezk, O. A. El-Gammal, S. H. Alrefaee, I. Althagafi, A. A. El-Bindary, M. A. El-Bindary, *Heliyon* **2023**, *9*, e21015.
[27] O. A. El-Gammal, A. A. El-Bindary, F. Sh. Mohamed, G. N. Rezk, M. A. El-Bindary, *Int. J. Liq.* **2022**, *346*, 117850.
[28] S. M. Abd-El-Hamid, A. S. Sadeek, N. B. Sadek, M. A. Sabry, M. S. El-Gedamy, *Int. J. Liq.* In Press **2024**.
[29] G. G. Mohamed, H. F. Abd El-Halim, M. M. I. El-Dessouky, W. H. Mahmoud, *J. Mol. Struct.* **2011**, *999*, 29–38.
[30] L. M. M. Vieira, M. V. de Almeida, M. C. S. Lourenço, F. A. F. M. Bezerra, A. P. S. Fontes, *Eur. J. Med. Chem.* **2009**, *44*, 4107–4111.
[31] M. M. Moawad, W. G. Hanna, *J. Coord. Chem.* **2002**, *55*, 439–457.
[32] H. S. Elshafie, S. A. Sadeek, I. Camele, A. A. Mohamed, *Int. J. Mol. Sci.* **2022**, *23*, 2110.
[33] S. Kumar, A. Rai, S. B. Rai, D. K. Rai, A. N. Singh, V. B. Singh, *J. Mol. Struct.* **2006**, *791*, 23–29.
[34] K. Nakamoto, *Infrared Spectra of Inorganic and Coordination Compounds*, Fourth ed., Wiely and Sons, New York, **1996**.
[35] W. M. I. Hassan, M. A. Badawy, G. G. Mohamed, H. Moustafa, S. Elramly, *Spectrochim. Acta Part A* **2013**, *111*, 169–177.
[36] T. A. Yousef, G. M. Abu El-Reash, O. A. El-Gammal, R. A. Bedier, *J. Mol. Str.* **2013**, *1035*, 307–317.
[37] A. Tarushi, G. Psomas, C. P. Raptopoulou, V. Psycharis, D. P. Kessissoglou, *Polyhedron.* **2009**, *28*, 3272–3278.
[38] M. A. El-Ghamry, A. A. Saleh, S. M. E. Khalil, A. A. Mohammed, *Spectrochim. Acta Part A* **2013**, *110*, 205–216.
[39] A. Tarushi, C. P. Raptopoulou, V. Psycharis, A. Terzis, G. Psomas, D. P. Kessissoglou, *Bioorg. Med. Chem.* **2010**, *18*, 2678–2685.
[40] I. Turel, *Coord. Chem. Rev.* **2002**, *232*, 27–47.
[41] G. G. Mohamed, N. E. A. El-Gamel, F. N. Nour El-Dien, *React. Inorg. Met. Org. Chem.* **2001**, *31*, 347–358.
[42] D. R. Zhu, Y. Song, Y. Xu, Y. Zhang, S. S. S. Raj, H. K. Fun, X. Z. You, *Polyhedron* **2000**, *19*, 2019–2025.
[43] H. F. Abd El-halim, M. M. Omar, G. G. Mohamed, *Spectrochim. Acta Part A* **2011**, *78*, 36–44.
[44] S. Yadav, R. V. Singh, *Spectrochim. Acta Part A* **2011**,*78*, 298–306.
[45] B. Macias, M. Martinez, A. Sanchez, A. A. Dominguez-Gil, *Int. J. Pharm.* **1994**, *106*, 229–235.
[46] N. Mondal, D. K. Dey, S. Mitra, K. M. Abdul Malik, *Polyhedron* **2000**, *19*, 2707–2711.
[47] T. A. Mohamed, I. A. Shaaban, R. S. Farag, W. M. Zoghaib, M. S. Afifi, *Spectrochim. Acta Part A* **2015**, *135*, 417–427.
[48] G. G. Mohamed, E. M. Zayed, A. M. Hindy, *Spectrochim. Acta Part A* **2015**, *145*, 76–84.
[49] G. G. Mohamed, N. E. A. El-Gamel, F. Teixidor, *Polyhedron* **2001**, *20*, 2689–2696.
[50] M. M. Rashad, A. M. Hassan, A. M. Nassar, N. M. Ibrahim, A. Mourtada, *Appl. Phys. A* **2013**, *117*, 877.
[51] J. Tauc, J. Mater, *Res. Bull.* **1968**, *3*, 37.
[52] F. Karipcin, B. Dede, Y. Caglar, D. Hur, S. Ilican, M. Caglar, Y. Sahin, *Opt. Commun.* **2007**, *272*, 131.
[53] S. K. Sengupta, O. P. Pandey, B. K. Srivastava, V. Sharma, *Transition Met. Chem.* **1998**, *23*, 349.
[54] N. Turan, B. Gündüz, H. Körkoca, R. Adigüzel, N. Çolak, K. Buldurun, *J. Mex. Chem. Soc.* **2014**, *58*, 65.
[55] T. S. Lobana, A. Sánchez, J. S. Casas, *J. Chem. Soc.* **1997**, *22*, 4289–4299.
[56] P. Drevensêk, J. Kosmrlj, G. Giester, T. Skauge, E. Sletten, K. Sepcìc, I. Turel, *J. Inorg. Biochem.* **2006**, *100*, 1755–1763.
[57] S. A. Sadeek, W. H. El-Shwiniy, W. A. Zordok, A. M. El-Didamony, *Spectrochim. Acta Part A* **2011**, *78*, 854–867.
[58] T. Stringer, P. Chellan, B. Therrien, N. D. T. Shunmoogam-Gounden Hendricks, G. S. Smith, *Polyhedron* **2009**, *28*, 2839–2846.
[59] E. K. Efthimiadou, Y. Sanakis, N. Katsaros, A. Karaliota, G. Psomas, *Polyhedron* **2007**, *26*, 1148.
[60] S. S. Alias, A. B. Ismail, A. A. Mohamad, *J. Alloys Compd.* **2010**, *499*, 231–237.
[61] E. K. Efthimiadou, N. Katsaros, A. Karaliota, G. Psomas, *Bioorg. Med. Chem. Lett.* **2007**, *17*, 1238.
[62] A. W. Coats, J. P. Redfern, *Nature* **1964**, *201*, 68–69.
[63] H. H. Horowitz, G. Metzger, *Traces. Anal. Chem.* **1963**, *35*, 1464–1468.
[64] O. A. El Gammal, *Inorg. Chim. Acta.* **2015**, *435*, 73–81.
[65] S. H. Sakr, H. S. Elshafie, I. Camele, S. A. Sadeek, *Molecules.* **2018**, *23*, 1182.
[66] N. H. Patel, H. M. Parekh, M. N. Patel, *Pharm. Chem. J.* **2007**, *1*, 78–81.

[67] F. I. Abouzayed, S. A. Abouel-Enein, A. M. Hammad, *ACS Omega.* **2021**, *15*, 27737–27754.
[68] Z. H. Chohan, K. M. Khan, C. T. Supuran, *Appl. Organomet. Chem.* **2004**, *18*, 305–310.
[69] H. S. Elshafie, L. De Martino, C. Formisano, L. Caputo, V. De Feo, I. Camele, *Plants* **2023**, *12*, 1869.
[70] H. S. Elshafie, I. Camele, R. Racioppi, L. Scrano, N. S. Iacobellis, S. A. Bufo, *Int. J. Mol. Sci.* **2012**, *13*, 16291–16302.
[71] F. Ceglie, H. S. Elshafie, V. Verrastro, F. Tittarelli, *J. Compost Sci. Util.* **2011**, *19*, 293–300.Manuscript received: December 12, 2023Version of record online: April 29, 2024

Manuscript received: December 12, 2023
Accepted manuscript online: April 29, 2024
Version of record online: ■■, ■■